NANO LETTERS

Letter

pubs.acs.org/NanoLett

Synthesis of Monolayer Hexagonal Boron Nitride on Cu Foil Using Chemical Vapor Deposition

Ki Kang Kim,[†] Allen Hsu,[†] Xiaoting Jia,[‡] Soo Min Kim,[†] Yumeng Shi,[†] Mario Hofmann,[†] Daniel Nezich,[†] Joaquin F. Rodriguez-Nieva,[‡] Mildred Dresselhaus,[†,§] Tomas Palacios,[†] and Jing Kong*[,†]

[†]Department of Electrical Engineering and Computer Sciences, [‡]Department of Materials Science and Engineering, and [§]Department of Physics, Massachusetts Institute of Technology, Cambridge, Massachusetts 02139, United States

Supporting Information

ABSTRACT: Hexagonal boron nitride (h-BN) is very attractive for many applications, particularly, as protective coating, dielectric layer/substrate, transparent membrane, or deep ultraviolet emitter. In this work, we carried out a detailed investigation of h-BN synthesis on Cu substrate using chemical vapor deposition (CVD) with two heating zones under low pressure (LP). Previous atmospheric pressure (AP) CVD syntheses were only able to obtain few layer h-BN without a good control on the number of layers. In contrast, under LPCVD growth, monolayer h-BN was synthesized and time-dependent growth was investigated. It was also observed that the morphology of the Cu surface affects the location and density of the h-BN nucleation. Ammonia borane is used as a BN precursor, which is easily accessible and more stable under ambient conditions than borazine. The h-BN films are characterized by atomic force microscopy, transmission electron microscopy, and electron energy loss spectroscopy analyses. Our results suggest that the growth here occurs via surface-mediated growth, which is similar to graphene growth on Cu under low pressure. These atomically thin layers are particularly attractive for use as atomic membranes or dielectric layers/substrates for graphene devices.

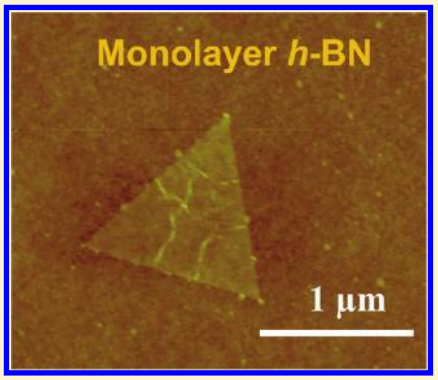

KEYWORDS: *Hexagonal boron nitride, chemical vapor deposition, ammonia borane, copper foil*

Hexagonal boron nitride (h-BN) is a III−V compound with a structure very similar to graphite and has been referred to as "white graphite". It is a layered structural material with a weak van de Waals interaction between the layers. Within each layer, its honeycomb structure is composed of alternating boron and nitrogen atoms instead of all carbon atoms, as in graphene.[1] While graphene/graphite is metallic/semimetallic in terms of its electrical properties, h-BN is an insulator with a direct band gap (5.97 eV).[2] Because of strong covalent sp^2 bonds in the plane, the in-plane mechanical strength and thermal conductivity of h-BN has been reported to be close to that of graphene, whereas h-BN has even higher chemical stability than graphene; it can be stable in air up to 1000 °C (in contrast, for graphene the corresponding temperature is ∼600 °C).[3−6] Similar to graphene, h-BN has a wide range of applications based on its remarkable properties, such as deep ultraviolet emitter, transparent membrane, dielectric layer, or protective coatings.[2,4,7] Recently, it has been highlighted that the on-substrate mobility of graphene on exfoliated single crystalline h-BN is comparable to that of suspended graphene due to its ultraflat and charge impurity-free surface.[8] Giant flexoelectric effect was also predicted for monolayer h-BN, suggesting its potential for ambient agitation energy harvesting.[9]

The growth of large area, few-layer h-BN films using chemical vapor deposition (CVD) on metallic substrates and transfer to other substrates has been reported in the past year.[5,10] Two different precursors have been used, ammonia-borane (H_3BNH_3, also called borazane)[5] or borazine ($B_3N_3H_6$),[10] both having a 1:1 B:N stoichiometry. Both methods used atmospheric pressure CVD (APCVD) synthesis and the resulting h-BN films are multilayer (5−50 nm).[10] Yet, the precise layer number control, down to a monolayer, was not achieved in the earlier works. Furthermore, the growth mechanism still remains uncertain.

Here, we report the growth of large area monolayer h-BN on Cu foil with h-BN synthesis under low pressure (LPCVD). An advantage of using LPCVD is that the growth is preferentially surface reaction limited and the results are less affected by the geometry of the substrate or gas flow effect.[11] Borazane is chosen as the precursor instead of borazine in this work, because of its stability in ambient and wider availability (in contrast, borazine is moisture-sensitive and hydrolyzes to boric acid, ammonia, and hydrogen).[12] Very interestingly, the initial flakes of h-BN are triangular instead of hexagonal as in the case of graphene. Another asymmetric diamond shape of the flakes was also observed. And with prolonged growth time, the flakes coalesce together forming a complete layer. In addition, it was found that the nucleation sites are influenced by the condition of the growth substrate.

Received: September 17, 2011
Revised: November 1, 2011
Published: November 23, 2011

   dx.doi.org/10.1021/nl203249a | *Nano Lett.* 2012, 12, 161−166

To synthesize monolayer h-BN on copper foil, a two-heating-zone system is installed to use borazane powder (Figure 1a). T_2

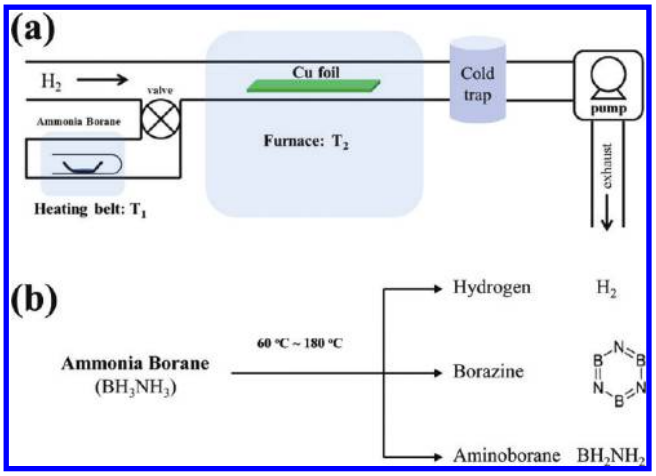

Figure 1. h-BN LPCVD setup and borazane decomposition. (a) The schematic diagram of hexagonal boron nitride (h-BN) LPCVD synthesis setup, T_2 temperature is fixed at 1000 °C for this study. (b) Ammonia borane is thermally decomposed to hydrogen, borazine, and amminoborane at 60∼180 °C.

temperature was fixed at 1000 °C in this study. At room temperature, borazane is a crystalline solid and melts around 106 °C.[13] In order to use it as a precursor for the CVD growth, the T_1 zone is heated up to generate borazane vapor from its solid and to diffuse the precursor into the T_2 zone. In APCVD synthesis using borazane as a precursor,[5] T_1 is set to 130 °C. In our experiments, we have found when T_1 is heated above borazane's melting temperature, there will be vigorous melting and reaction. In fact it has been shown previously that thermally activated decomposition of borazane takes place in the temperature range 77−137 °C accompanied by hydrogen release and heat evolution,[13] and under appropriated conditions, borazane can decompose completely below its melting temperature. The decomposition of borazane produces hydrogen, monomeric aminoborane (BH_2NH_2) and borazine ($(HBNH)_3$ (Figure 1b).[12,14,15] Monomeric aminoborane (BH_2NH_2) is very active and it forms polymeric aminoborane (BH_2NH_2), which is a white noncrystalline solid and stable at room temperature. Therefore, the synthesis of h-BN using a borazane source is relatively complicated; the precursor should be a mixture of borazane, aminoborane, and borazine. In our LPCVD, we have found that T_1 between 60−90 °C is sufficient for h-BN growth.

Additional changes to the furnace were required due to the transition to growth at low pressure. It was found that having a carrier gas flowing through T_1 zone (as in the case of APCVD) is not proper to obtain clean monolayer h-BN. When a carrier gas flows through T_1, very often particles 50−100 nm in diameter are observed on the Cu surface (see Supporting Information Figure S1). The particle density is much higher when T_1 is above 100 °C (see Supporting Information Figure S1a,b). Under transmission electron microscopy (TEM), hollow nanospheres of similar sizes are observed together with the h-BN film (see Supporting Information Figure S1c,d). The growth of BN nanoparticle/hollow nanospheres via vapor phase pyrolysis of borazane has been reported,[16] we suspect that in our samples, BN nanospheres are formed in zone T_1. Therefore in the present version of our CVD setup (Figure 1a), there is no carrier gas flowing through zone T_1 and the precursors enter the growth zone T_2 by diffusion. Presumably heavier particles like the nanospheres (see Supporting Information Figure S1) will not diffuse far enough to reach the growth substrate. Indeed, this is what we found; clean h-BN surfaces free of particles can be obtained in this way under LPCVD.

Clean monolayer h-BN obtained by the optimized setup was transferred onto a 300 nm SiO_2/Si, quartz substrate, and TEM grid to characterize the number of layers and their crystallinity. As the optical contrast of monolayer h-BN on 300 nm SiO_2/Si is very small,[17] it is hard to distinguish between monolayer h-BN and SiO_2 by optical microscopy (Figure 2a). Only some impurities at the edge of the film help to recognize the boundary, as indicated by white dotted line in Figure 2a. The inset in Figure 2a displays the characteristic of "white graphene" monolayer h-BN (red dotted square), presenting very high transparency. To confirm the existence of monolayer h-BN on the quartz substrate, it was analyzed by the optical absorption (Figure 2b). In the visible range, almost zero absorbance was detected for h-BN in contrast to the graphene case. In the UV range, while graphene has π plasmon peak around 4.6 eV,[18] the interband transitions associated with high joint density of states for monolayer h-BN were observed at 6.16 eV.[19] The optical band gap (OBG) of monolayer h-BN can be obtained using the formula for a direct band semiconductor. From previous works,[10,20] the absorption coefficient is given as $\alpha = C(E - E_g)^{1/2}/E$, where C is a constant and E_g is the OBG. Therefore, the power law behavior of $(\alpha E)^2 \propto (E - E_g)$ can be obtained. The plot of $(\alpha E)^2$ versus E should then give a straight line, and when $(\alpha E)^2 = 0$ the corresponding E value should be equal to E_g. The OBG of monolayer h-BN in this work is found to be 6.07 eV (see Supporting Information Figure S2). This value is slightly larger than that of bulk h-BN or few layer h-BN, which can be attributed to the fact that there is no layer−layer interaction.[5,10,19] In fact, this value is closer to the band gap value predicted by theoretical calculation (6.0 eV).[21]

To elucidate the growth of monolayer h-BN, the sample was characterized by TEM and atomic force microscopy (AFM). The TEM image of monolayer h-BN clearly demonstrated that the number of layer of h-BN is one (Figure 2c). Figure 2d shows the AFM image of the h-BN flakes (via short growth time) transferred to a SiO_2/Si substrate; here sharp edges of the flakes can be seen (indicated by white arrows). The inset of Figure 2d indicates that the typical thickness of h-BN is less than 0.420 nm, consistent with monolayer growth (c-axis spacing for h-BN is ∼0.32 nm). Furthermore, we found that the surface roughness (for areas without wrinkles) is about 0.181 nm, which is smoother than that of the silicon dioxide (0.222 nm) substrate that the h-BN is sitting on (see Supporting Information Figure S3). Both the sharp edge and the smooth surface suggest the high structural quality of the h-BN monolayer. For a complete h-BN layer (Figure 2e), the wrinkles of the h-BN film (indicated by a yellow arrow) under scanning electron microscopy (SEM) can be clearly seen. These wrinkles are characteristic of h-BN and graphene films due to the negative thermal expansion coefficients of h-BN and graphene (i.e., since the h-BN layer is grown on the Cu at high temperature, when the substrate is cooled to room temperature, the Cu shrinks but the h-BN expands, resulting in wrinkles).[22] In addition, the surface of h-BN on Cu foil looks quite clean. We have found that SEM is very useful to characterize h-BN on Cu foil.

dx.doi.org/10.1021/nl203249a | Nano Lett. 2012, 12, 161−166

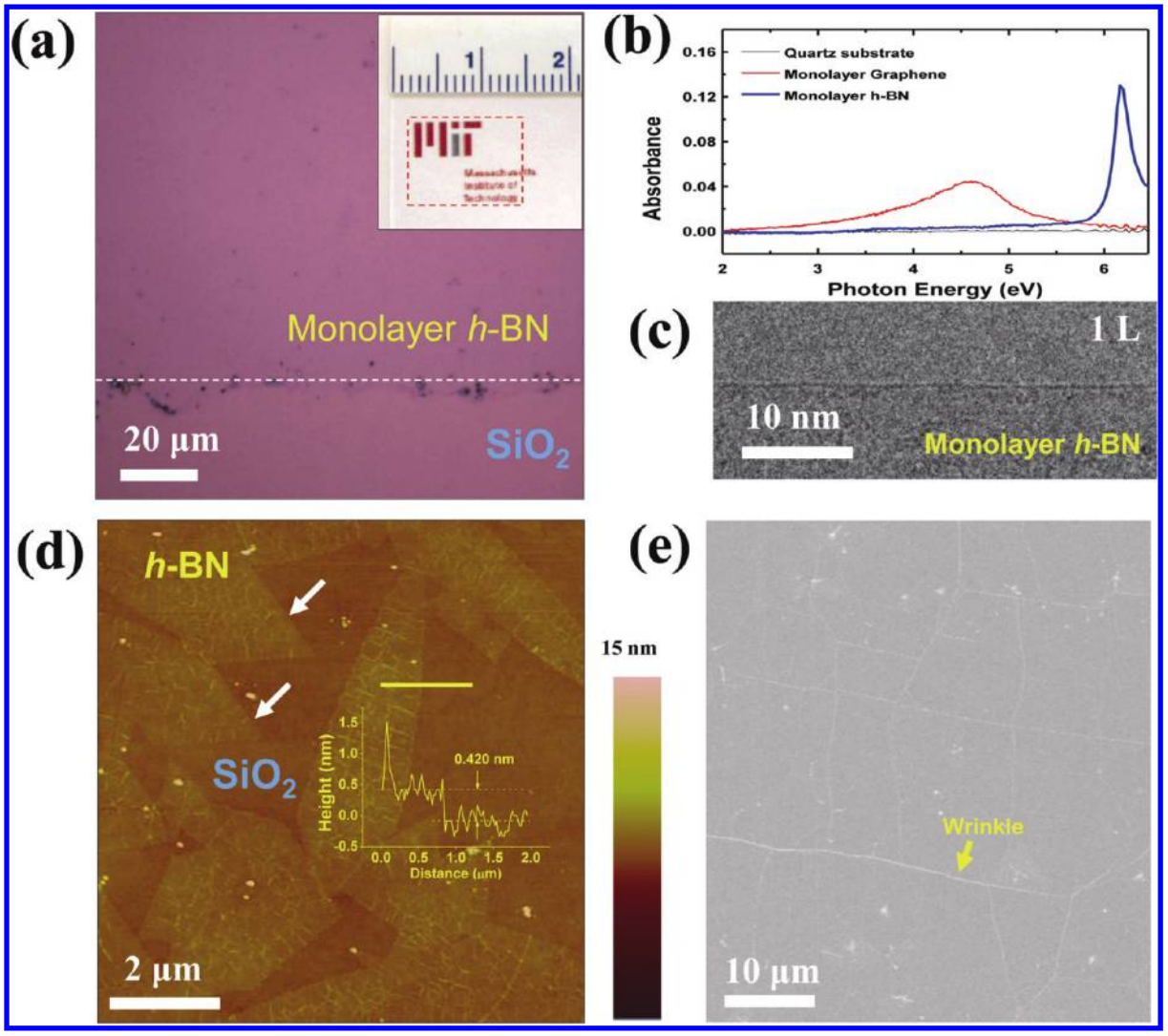

Figure 2. Monolayer h-BN characterization. (a) Optical image of h-BN on 300 nm SiO_2/Si. White dotted line indicates the border between h-BN and SiO_2. The inset displays a photograph of h-BN film on a quartz substrate (red dotted area), showing high transparency. (b) Optical absorption spectra of a monolayer h-BN, monolayer graphene and a quartz substrate (as a reference). (c) TEM image of the folded edge of a monolayer h-BN. (d) AFM images of the initial flakes of the h-BN. The white arrows point to the sharp edges of these flakes. The inset indicates the height distribution along the yellow line in (d). (e) SEM image of a continuous monolayer h-BN. The yellow arrow indicates one of the h-BN wrinkles.

The monolayer h-BN was further characterized by selective area electron diffraction pattern (SAED) and electron energy loss spectroscopy (EELS) in TEM and X-ray photoemission spectroscopy (XPS) (see Supporting Information Figures S4 and S5). Single hexagonal diffraction pattern in small area (<1600 nm^2) and more than two hexagonal diffraction patterns in larger area (>4 μm^2) were observed, indicating that monolayer h-BN is hexagonal in structure but has multiple domains for >4 μm^2 region. To estimate the boron and nitrogen bonding nature and the stoichiometry of h-BN, the sample was characterized by EELS. It is clearly shown that both the π^* and σ^* energy-loss peaks at the boron K-shell (near 180 eV) are present, indicating that h-BN has sp^2 hybridization bonds.[23] In addition, the stoichiometry of boron and nitrogen was obtained to be 45:55 after integration of each characteristic peak.

To understand the growth mechanism, we carried out systematic studies in terms of nucleation, and growth. For the study of nucleation on Cu surface, the T_1 temperature was varied from 60 to 90 °C with a fixed growth time of 10 min. Unlike hexagonal island of graphene on Cu foil,[24] the nucleation islands of h-BN under 60 °C T_1 temperature has triangular shapes (Figure 3a). This triangle shape was observed by the growth of h-BN on Ni(111) with precursors of borazine and B-trichloroborazine,[25,26] which is attributed to less lattice mismatch (−0.4%) between Ni(111) and h-BN.[27] As Cu(111) is also face-centered cubic (fcc) (same as Ni) with similar lattice constant as Ni (the lattice mismatch with between Cu and h-BN is +2%), it is expected that similar behavior will occur. While the triangle islands on Ni(111) are well-oriented on Ni(111), the triangle islands obtained in this work are typically randomly oriented even within the same Cu grain (Figure 3a and inset) except for a few cases (see Supporting Information Figure S6). Previous work explained that an h-BN monolayer on Ni(111) is found to be strongly chemisorbed, but on Cu(111) it is weakly chemisorbed due to the different chemical bonding at the interface.[27] Thus, it is likely due to this reason that the growth of h-BN flakes on Cu do not have a preferred orientation.

dx.doi.org/10.1021/nl203249a | Nano Lett. 2012, 12, 161−166

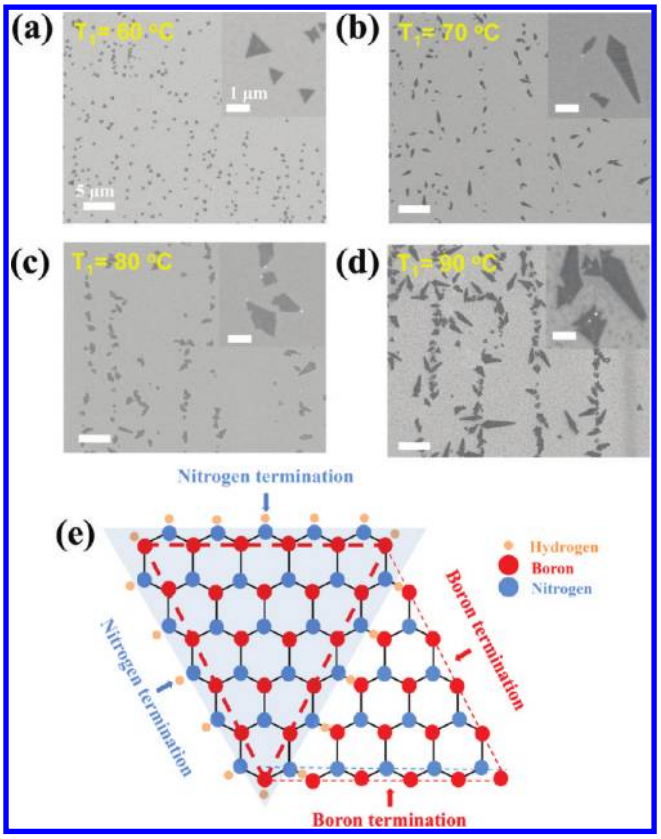

Figure 3. The T_1 temperature dependence of h-BN growth for 10 min. SEM images of (a) 60, (b) 70, (c) 80, and (d) 90 °C of T_1 temperature, respectively. The inset of each figure shows higher magnification. (e) Schematic illustration of a nitrogen-terminated h-BN triangle, the triangle next to it can only have boron-termination at the edges.

Regarding the triangular shape of the flakes, it has been reported that the edges of the triangle islands on Ni(111) are nitrogen-terminated, based on both experimental results and theoretical calculations,[25,26] because the nitrogen-terminated triangles have lower edge energy than that of the boron-terminated ones.[28] Figure 3e illustrates a nitrogen-terminated triangular island. It turns out that the next triangle must be a boron-terminated triangle from simple geometry, and if a hexagonal flake of h-BN is formed by this way, the edges need to be nitrogen-terminated and boron-terminated alternating with each other. From the previous discussions, this would be energetically unfavorable as boron-terminated edge will cost more energy. Therefore this suggests why our h-BN flakes are triangular in shape instead of hexagonal as observed in the case of graphene. In fact the growth of hexagonal flakes of h-BN has never been observed in our experiments or reported in the literature.

For higher T_1 temperatures, asymmetric diamond shapes of h-BN flakes were observed to be dominant (Figure 3b–d). Quite often one side of the diamond is an equilateral triangle (see Supporting Information Figure S7) similar to islands in Figure 3a and is likely to be nitrogen-terminated on the edge. For the other side of the diamond, the two edges have to be terminated by both nitrogen and boron. We have never observed diamond shapes having two equilateral triangles next to each other, which supports our previous hypothesis that the boron-terminated edges might be too energetically unfavorable for this to happen. We have also observed other variations of the asymmetric diamond shape (see Supporting Information Figure S7). In addition, white particles are frequently observed at the end of the longer side of the asymmetric diamond. At this stage, the nature of the white particle and the reason for such asymmetric diamond shape is still not fully understood yet.

h-BN syntheses with different periods of time were also carried out to elucidate how the growth progresses. Figure 4

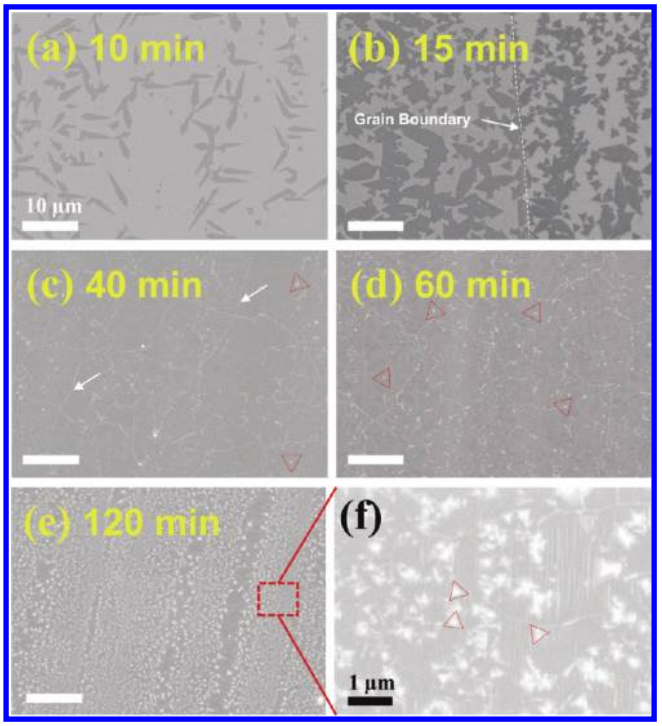

Figure 4. Growth time dependence with T_1 = 70 °C. SEM images of (a) 10, (b) 15, (c) 40, (d) 60, and (e) 120 min in growth time, respectively. (f) Higher magnification of the dotted square region in (e). The dotted red triangles indicate the multilayered h-BN region.

shows the SEM images of h-BN on Cu grown under the same condition under 10, 15, 40, 60, and 120 min of growth time. Comparing the 15 min growth result with the 10 min result, it appears that the initial flakes are increased both in size (area) and density (i.e., more nucleation sites come out) for longer growth times. Both the triangular shape and the asymmetric diamond shape were observed as the initial form of the flakes. h-BN flakes growing across Cu grain boundaries were also observed frequently. A similar observation has been reported for graphene growth on Cu foil. This suggests that h-BN growth in LPCVD is surface-mediated (Figure 4b).[24,29,30] By 40 min the monolayer growth is almost complete and an open Cu surface can hardly be found under SEM. On the other hand, characteristic wrinkles are observed on the surface. Furthermore, sites with multiple layers appear, as outlined by the red triangles (a zoomed in image is shown in Figure 4f). With even longer growth periods (60 and 120 min), these multilayer sites increase in density (Figure 4d,e). After 120 min growth, the surface was mostly covered by multilayers of triangles. From TEM analysis, we confirmed that the background layer of h-BN is mostly monolayer with triangular multilayer regions. Thus it appears that under our current LPCVD conditions, the h-BN growth follows the Frank van der Merwe model (i.e., layer-by-layer growth) for the first layer, presumably due to the strong adatom-surface (Cu) interaction, but changes to Stranski-

dx.doi.org/10.1021/nl203249a | Nano Lett. 2012, 12, 161–166

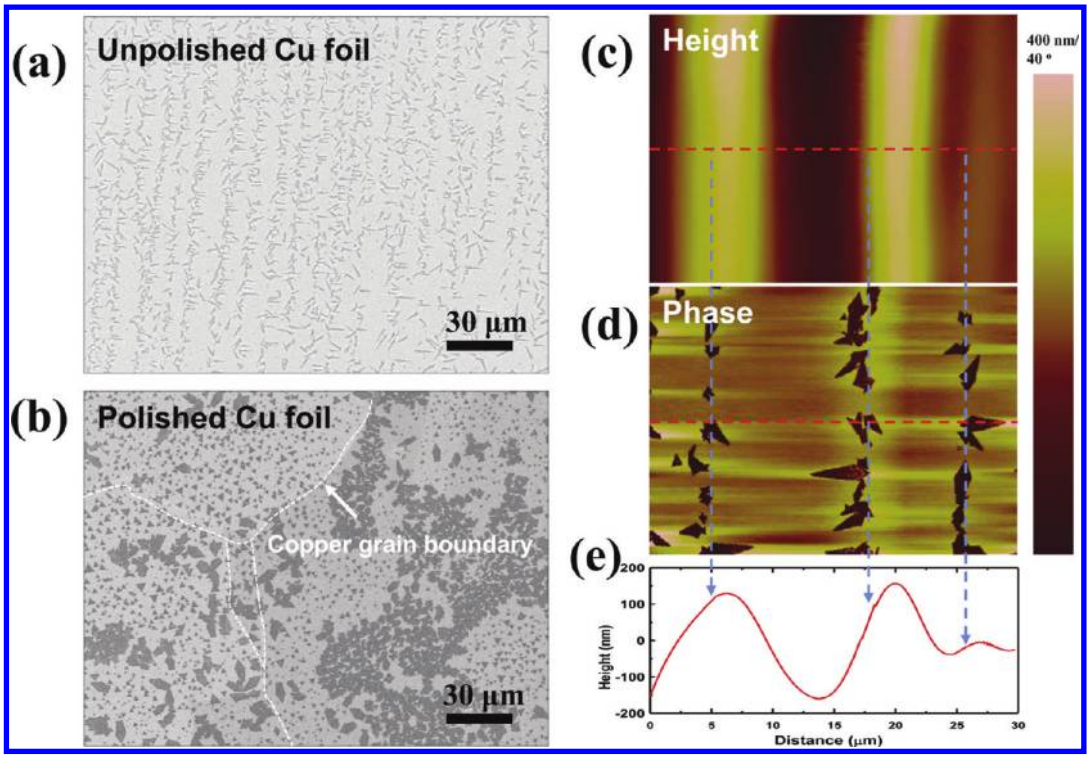

Figure 5. Effect of copper surface morphology on h-BN growth. SEM images of (a) an unpolished copper foil and (b) a polished copper foil after h-BN growth for 10 min with T_1 = 70 °C. (c,d) AFM images of the unpolished copper foil after growth for (c) height and (d) phase images. (e) Height profile along the red dotted in (c) and (d).

Krastanov model (i.e., island on layer) after the first layer.[31,32] To a certain extent, this behavior is similar to the growth of graphene on Cu under LPCVD except the fact that the presence of the multilayer sites and their development with time suggest the growth of h-BN on Cu under such LPCVD is not self-limited, which is in contrast to the case of graphene.

Under the current LPCVD growth conditions we also found that quite often the surface morphologies affects the nucleation of the growth. This behavior can be seen in the SEM image of a typical short time (10 min) growth result in Figure 5a. The nucleation mostly occurs along the copper rolling line, which gives rise to an interesting pattern in the SEM image (Figure 5a). In order to distinguish whether h-BN nucleates on the groove or on a hill region of the copper foil, the height profile and phase image under AFM are compared; this comparison revealed that the nucleation occurs on one side of the hill. Considering the growth is carried out under LPCVD where the growth rate is limited by surface reaction, the higher nucleation density should not be caused by any gas flow effect, for example, possible pressure difference between the hill side facing the flow versus the hill side away from flow or between the hill and valley regions. Rather, it is likely there are more impurity sites on the Cu surface along the rolling lines, which induce the nucleation of h-BN, similar to the graphene case.[33] However, it is unclear why the nucleation only occurs on one side of the hill. Very interestingly, we found that when the copper surface is polished by the electrochemical polishing (ECP) method[34] (which results in a very smooth and flat surface), the nucleation sites are more evenly distributed on the Cu surface (Figure 5b). Furthermore, the average size of the triangular island is larger than that of the unpolished copper surface. This suggests the possibility of using a polished Cu surface to grow h-BN films with larger single crystalline domains.

In conclusion, we present in this work the LPCVD synthesis to obtain large area monolayer h-BN films. Such synthesis conditions allow the observation of the h-BN nucleation and extension processes. Unlike the hexagonal shape of graphene nucleation islands,[24] h-BN starts to grow with a triangular shape, possibly due to the more energetically favored nitrogen-terminated edges. Another interesting asymmetric diamond shape is also observed, and the origin of this shape is unclear at this stage. With prolonged growth, the flakes extend in area and merge with each other resulting in a complete layer covering the Cu surface. We have also found that the morphology of the Cu surface affect the location and density of the h-BN flakes, which points to the potential of engineering the Cu substrate to control the growth of h-BN in the future.

■ ASSOCIATED CONTENT

Ⓢ Supporting Information

Method details and Figures S1−S7. This material is available free of charge via the Internet at http://pubs.acs.org.

■ AUTHOR INFORMATION

Corresponding Author

*E-mail: jingkong@mit.edu.

■ ACKNOWLEDGMENTS

This work is partially supported by the National Science Foundation under award number NSF DMR 0845358 and the Materials, Structures and Device (MSD) Center, one of the five programs in the focus center research program (FCRP), a Semiconductor Research Corporation program. D.N. and A.H. acknowledge the support from MIT/Army Institute for Soldier

Nanotechnologies (ISN). M.H., X.J., M.S.D., and J.K. acknowledge the Graphene Approaches to Terahertz Electronics (GATE) - MURI Grant N00014-09-1-1063.

REFERENCES

(1) Pease, R. S. *Nature* **1950**, *165* (4201), 722−723.
(2) Kubota, Y.; Watanabe, K.; Tsuda, O.; Taniguchi, T. *Science* **2007**, *317* (5840), 932−934.
(3) Kho, J. G.; Moon, K. T.; Kim, J. H.; Kim, D. P. *J. Am. Ceram. Soc.* **2000**, *83* (11), 2681−2683.
(4) Sugino, T.; Tai, T. *Jpn. J. Appl. Phys., Part 2* **2000**, *39* (11A), L1101−L1104.
(5) Song, L.; Ci, L.; Lu, H.; Sorokin, P. B.; Jin, C.; Ni, J.; Kvashnin, A. G.; Kvashnin, D. G.; Lou, J.; Yakobson, B. I.; Ajayan, P. M. *Nano Lett.* **2010**, *10* (8), 3209−15.
(6) Chen, Y.; Zou, J.; Campbell, S. J.; Le Caer, G. *Appl. Phys. Lett.* **2004**, *84* (13), 2430−2432.
(7) Watanabe, K.; Taniguchi, T.; Kanda, H. *Nat. Mater.* **2004**, *3* (6), 404−409.
(8) Dean, C. R.; Young, A. F.; Meric, I.; Lee, C.; Wang, L.; Sorgenfrei, S.; Watanabe, K.; Taniguchi, T.; Kim, P.; Shepard, K. L.; Hone, J. *Nat. Nanotechnol.* **2010**, *5* (10), 722−726.
(9) Naumov, I.; Bratkovsky, A. M.; Ranjan, V. *Phys. Rev. Lett.* **2009**, *102* (21), 217601.
(10) Shi, Y. M.; Hamsen, C.; Jia, X. T.; Kim, K. K.; Reina, A.; Hofmann, M.; Hsu, A. L.; Zhang, K.; Li, H. N.; Juang, Z. Y.; Dresselhaus, M. S.; Li, L. J.; Kong, J. *Nano Lett.* **2010**, *10* (10), 4134−4139.
(11) Bhaviripudi, S.; Jia, X. T.; Dresselhaus, M. S.; Kong, J. *Nano Lett.* **2010**, *10* (10), 4128−4133.
(12) Wolf, G.; Baumann, J.; Baitalow, F.; Hoffmann, F. P. *Thermochim. Acta* **2000**, *343* (1−2), 19−25.
(13) Hu, M. G.; Geanangel, R. A.; Wendlandt, W. W. *Thermochim. Acta* **1978**, *23* (2), 249−255.
(14) Baitalow, F.; Baumann, J.; Wolf, G.; Jaenicke-Rossler, K.; Leitner, G. *Thermochim. Acta* **2002**, *391* (1−2), 159−168.
(15) Baumann, J.; Baitalow, E.; Wolf, G. *Thermochim. Acta* **2005**, *430* (1−2), 9−14.
(16) Wang, Y. T.; Yamamoto, Y.; Kiyono, H.; Shimada, S. *J. Am. Ceram. Soc.* **2009**, *92* (4), 787−792.
(17) Gorbachev, R. V.; Riaz, I.; Nair, R. R.; Jalil, R.; Britnell, L.; Belle, B. D.; Hill, E. W.; Novoselov, K. S.; Watanabe, K.; Taniguchi, T.; Geim, A. K.; Blake, P. *Small* **2011**, *7* (4), 465−468.
(18) Nair, R. R.; Blake, P.; Grigorenko, A. N.; Novoselov, K. S.; Booth, T. J.; Stauber, T.; Peres, N. M. R.; Geim, A. K. *Science* **2008**, *320* (5881), 1308−1308.
(19) Hoffman, D. M.; Doll, G. L.; Eklund, P. C. *Phys. Rev. B* **1984**, *30* (10), 6051.
(20) Yuzuriha, T. H.; Hess, D. W. *Thin Solid Films* **1986**, *140* (2), 199−207.
(21) Blase, X.; Rubio, A.; Louie, S. G.; Cohen, M. L. *Phys. Rev. B* **1995**, *51* (11), 6868.
(22) Yates, B.; Overy, M. J.; Pirgon, O. *Philos. Mag.* **1975**, *32* (4), 847−857.
(23) Huang, J. Y.; Yasuda, H.; Mori, H. *J. Am. Ceram. Soc.* **2000**, *83* (2), 403−409.
(24) Yu, Q. K.; Jauregui, L. A.; Wu, W.; Colby, R.; Tian, J. F.; Su, Z. H.; Cao, H. L.; Liu, Z. H.; Pandey, D.; Wei, D. G.; Chung, T. F.; Peng, P.; Guisinger, N. P.; Stach, E. A.; Bao, J. M.; Pei, S. S.; Chen, Y. P. *Nat. Mater.* **2011**, *10* (6), 443−449.
(25) Auwarter, W.; Suter, H. U.; Sachdev, H.; Greber, T. *Chem. Mater.* **2004**, *16* (2), 343−345.
(26) Auwarter, W.; Muntwiler, M.; Osterwalder, J.; Greber, T. *Surf. Sci.* **2003**, *545* (1−2), L735−L740.
(27) Preobrajenski, A. B.; Vinogradov, A. S.; Martensson, N. *Surf. Sci.* **2005**, *582* (1−3), 21−30.
(28) Liu, Y.; Bhowmick, S.; Yakobson, B. I. *Nano Lett.* **2011**, *11* (8), 3113−6.
(29) Li, X. S.; Cai, W. W.; An, J. H.; Kim, S.; Nah, J.; Yang, D. X.; Piner, R.; Velamakanni, A.; Jung, I.; Tutuc, E.; Banerjee, S. K.; Colombo, L.; Ruoff, R. S. *Science* **2009**, *324* (5932), 1312−1314.
(30) Li, X. S.; Cai, W. W.; Colombo, L.; Ruoff, R. S. *Nano Lett.* **2009**, *9* (12), 4268−4272.
(31) Pimpinelli, A.; Villain, J. Cambridge University Press: New York, 1998.
(32) Venables, J. A. Cambridge University Press: New York, 2000.
(33) Vlassiouk, I.; Regmi, M.; Fulvio, P.; Dai, S.; Datskos, P.; Eres, G.; Smirnov, S. *ACS Nano* **2011**, *5* (7), 6069−6076.
(34) Aksu, S. *J. Electrochem. Soc.* **2009**, *156* (11), C387−C394.